Supporting Information

Utilizing spent Li-ion batteries to regulate the π-conjugated structure of g-C₃N₄:

a win-win approach for waste recycling and highly-active photocatalyst

construction

Bo Niu[1], Jiefeng Xiao[1] and Zhenming Xu[1, 2]*

[1]School of Environmental Science and Engineering, Shanghai Jiao Tong University,

800 Dongchuan Road, Shanghai 200240, People's Republic of China

[2]Shanghai Institute of Pollution Control and Ecological Security, Shanghai 200092,

People's Republic of China

Corresponding author:

Zhenming Xu

Tel: +86 21 5474495; Fax: +86 21 5474495;

E-mail: zmxu@sjtu.edu.cn

1.1. Characterization

X-ray diffraction (XRD) measurements were performed on a D8-ADVANCE instrument with Cu Kα radiation. Fourier transform infrared (FTIR) spectra were recorded on a Nicolet6700 spectrophotometer. X-ray photoelectron spectroscopy (XPS) were obtained by AXIS UltraDLD. The UV-vis absorption spectra were obtained using a Lambda 950 UV/VIS/NIR spectrophotometer. Nitrogen adsorption-desorption isotherms were collected on a Quadrasorb SI at liquid N_2 temperature. The photoluminescence (PL) spectra were recorded on a RF5301PC spectrometer. Scanning electron microscope (Ultra-high resolution SEM, GAIA3) coupled with TOF-SIMS was used to characterize the morphology and microstructure of the samples.

1.2. Photoelectrochemical measurements

The photocurrent response (I-t) and electrochemical impedance (EIS) measurements were conducted with a CHI 660c electrochemical workstation in a conventional three electrode system. The Pt plate was used as the counter electrode and Ag/AgCl was used as the reference electrode. The electrolyte was 0.5 M Na_2SO_4 aqueous solution. The working electrode was prepared as follows [1]: 0.1 g photocatalyst and 0.01 g ethyl cellulose were mixed in ethanol to make a fine slurry. The slurry was coated onto an indium-tin oxide glass by a doctor blading method and then dried at 80 ºC for 2 h. The simulated sunlight came from a 300W Xe lamp with an AM 1.5 cutoff filter. For EIS measurements, the perturbation signal was 10 mV and the frequency ranged from 100 kHz to 10 mHz. The applied potential was 0.6 V vs Ag/AgCl for the I-t and EIS experiments. Mott-Schottky plots were measured using the

same electrolyte. The ac amplitude was 5mV and the frequency was 1 kHz.

1.3. Photocatalytic activity experiments

The photocatalytic H_2 evolution experiments were conducted in a quartz device (LabSolar-IIIAG, Perfect Light, China). 0.1 g catalyst was dispersed in 100 ml of aqueous solution (10 vol% triethanolamine). Then, the solution was degassed and irradiated with a 300 W Xe lamp with an AM 1.5 cutoff filter as the simulated sunlight source. Magnetic stirring of the solution was maintained through the experiment. The photocatalytic H_2 evolution rate was quantified by using an online gas chromatograph (GC2010plus, Japan, Ar as carrier gas). The recyclable photocatalytic activity tests were also performed, and the photocatalyst was collected by centrifugation after each run and used for next run.

The photocatalytic RhB degradation activities of various photocatalysts were also evaluated. 0.05 g catalyst was suspended in 50 mL of RhB solution (10 mg/l). The mixture was magnetically stirred for 60 min in dark to reach complete adsorption/desorption equilibrium. Then, the suspension solution was irradiated under simulated sunlight irradiation using a 300 W Xe lamp with an AM 1.5 cutoff filter. At the given time, 3 mL of the suspension were withdrawn from the reactor and analyzed by a UV-vis spectrophotometer (Perkin-Elmer, USA). To probe the active species in the photocatalysis, triethanolamine (TEOA, 1 mM), 1, 4-benzoquinone (BQ, 1 mM) and isopropyl alcohol (IPA, 1 mM) for RhB degradation were conducted. The trapping experiments were like the photodegradation experiment except that a quantity of scavengers was added to the RhB solution prior to adding photocatalyst. In addition,

the photocatalytic stability of photocatalyst was also evaluated by performing cycle runs. The photocatalyst was collected by centrifugation after each run and washed with deionized water several times, and dried for the next run.

1.4. DFT calculation

The DFT computations were conducted using the Vienna ab initio Simulation Package (VASP) code with a projector augmented wave (PAW) method [2-4]. The exchange-correlation function used the Perdew-Burke-Ernzerhof (PBE) [5, 6]. The energy cutoff was set 500 eV. Ionic relaxations were carried out until the atomic forces were converged to 0.05 eV/Å. The van der Waals (vdW) correction was included by using the DFT-D2 calculations [7]. Spin-polarized was used in the Li-Cl-Co regulated $g\text{-}C_3N_4$. We first relaxed a $1 \times 1 \times 2$ supercell of bulk $g\text{-}C_3N_4$. The obtained lattice constants were a = 7.12 Å, b = 7.12 Å and c = 12.61 Å, which well agreed with the previous results [8, 9]. Then, Li-Cl-Co atoms were introduced in interstitial (cave and interlayer) according to the previous studies [10-12]. By structure optimization, the Co was in the cave position (among the adjacent tri-s-triazine units) and Cl and Li were in the interlayer position. After obtaining the stable structure, the electronic structure was further calculated. The $4\times4\times2$ and $5\times5\times3$ k-points were applied in the structure optimization and electronic property calculations, respectively.
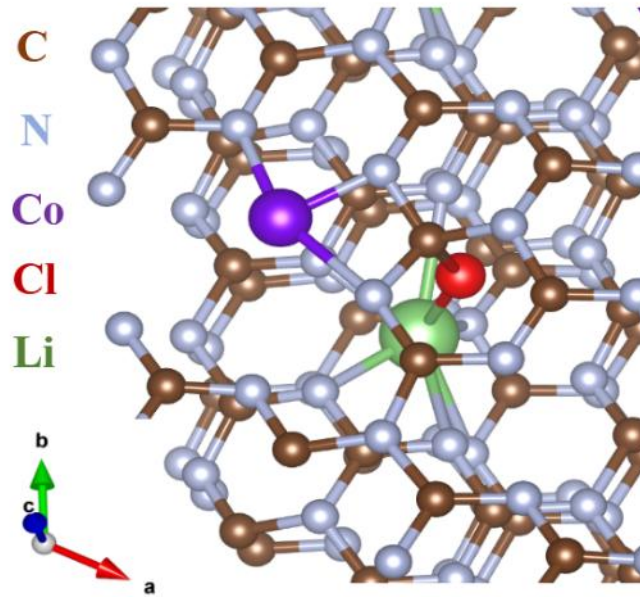
Fig. S1. The top side view of stable LiClCo-C3N4 structure after DFT calculation (It clearly that the Li, Cl and Co were stabilized in g-C$_3$N$_4$ through Co-N, Cl-C, Cl-Li and Li-N bonds)
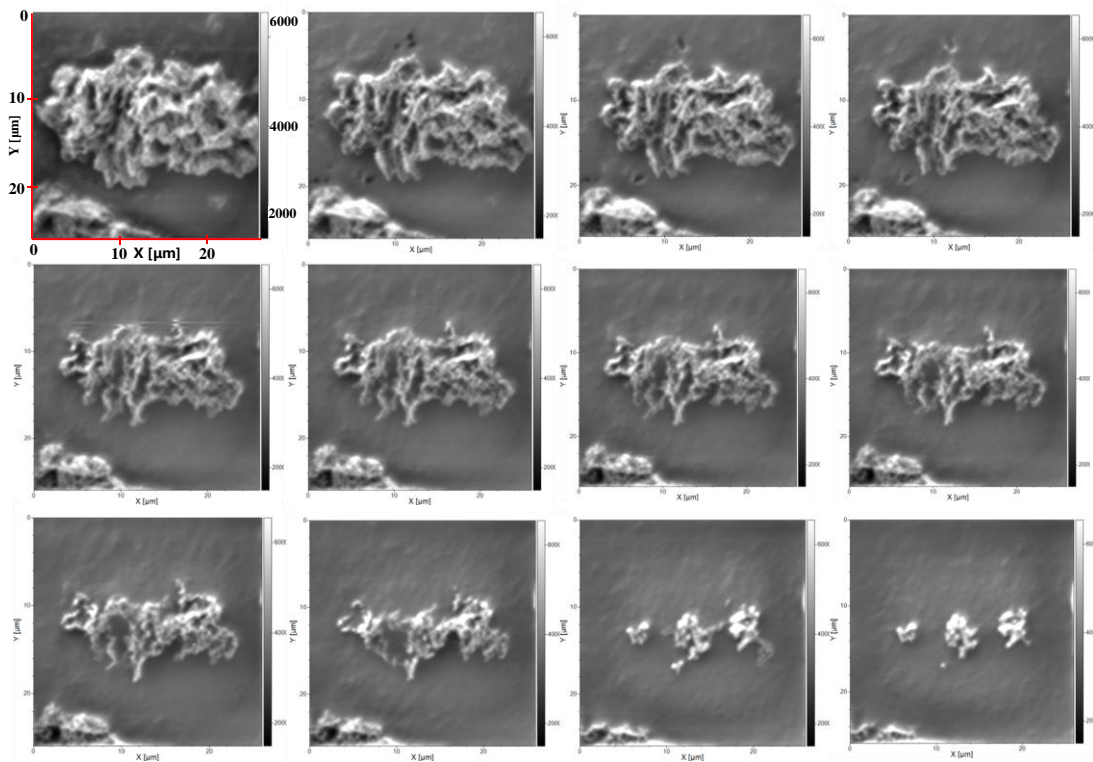

Fig. S2. The typical images for the select area to simultaneously detect the Li and Co

elements during the TOF-SIMS examining process (the area was gradually destroyed).

The coordinate dimensions of the other images were the same as those of the first image.
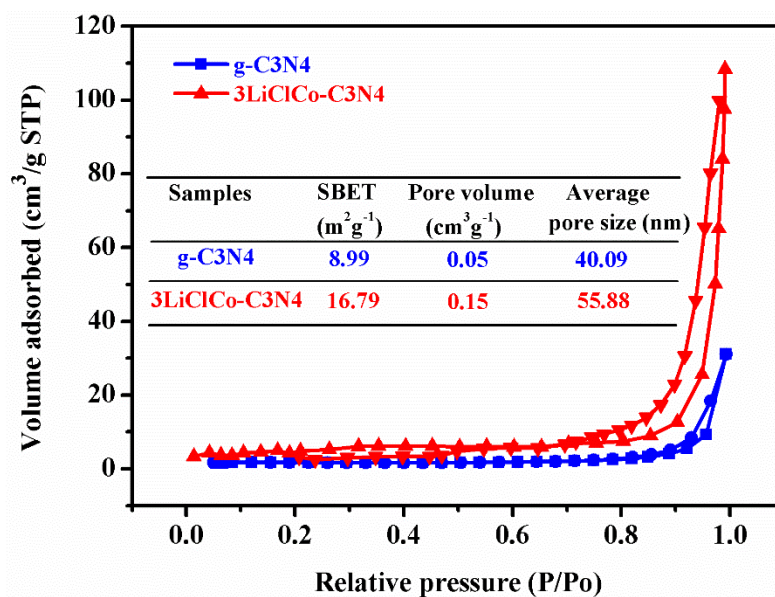

Samples	SBET $(m^2 g^{-1})$	Pore volume $(cm^3 g^{-1})$	Average pore size (nm)
g-C3N4	8.99	0.05	40.09
3LiClCo-C3N4	16.79	0.15	55.88

Fig. S3. The nitrogen sorption isotherm curves and the obtained S_{BET}, pore volume and average pore size of the samples
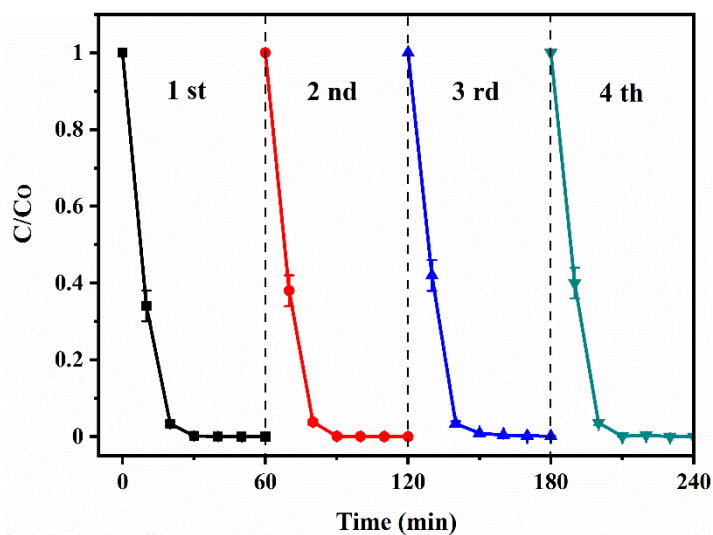

Fig. S4. The recyclable photocatalytic activity for RhB degradation.

Table S1 Recent studies on anion or cation doped g-C$_3$N$_4$ photocatalysts for H$_2$ evolution.

Photocatalyst	Performance compared to g-C$_3$N$_4$	Reaction condition [a]	Reference (Year)
O doped g-C$_3$N$_4$	5.2 times higher than that of g-C$_3$N$_4$	300 W, λ >400, TEOA	[13] (2016)
P doped g-C$_3$N$_4$/Ag$_3$PO$_4$	2.1 times higher than that of g-C$_3$N$_4$	300 W, simulated sunlight, methanol	[14] (2020)
Na-P doped g-C$_3$N$_4$	2.2 times higher than that of g-C$_3$N$_4$	350 W, methanol	[15] (2017)
K doped g-C$_3$N$_4$	5.4 times higher than that of g-C$_3$N$_4$	300 W, λ>400, TEOA	[16] (2018)
C doped g-C$_3$N$_4$	6.6 times higher than that of g-C$_3$N$_4$	300 W, λ>420 TEOA	[17] (2020)
B-F doped g-C$_3$N$_4$	5 times higher than that of g-C$_3$N$_4$	300 W, TEOA monochromatic light	[18] (2018)
Eu doped g-C$_3$N$_4$	7.3 times higher than that of g-C$_3$N$_4$	300 W, TEOA	[19] (2019)
K$^+$ and cyano decorated g-C$_3$N$_4$	12 times higher than that of g-C$_3$N$_4$	300 W, λ>420 TEOA	[20] (2020)
Co doped g-C$_3$N$_4$/MoS$_2$	4.7 times higher than that of g-C$_3$N$_4$	300 W, simulated sunlight, TEOA	[21] (2019)
Li-Cl-Co doped g-C$_3$N$_4$	**12.6 times higher than that of g-C$_3$N$_4$**	**300 W, simulated sunlight, TEOA**	**This work**

Note: (a) the light source was a Xenon-arc lamp.

Table S2 Recent studies on anion or cation doped g-C$_3$N$_4$ photocatalysts for RhB degradation

Photocatalyst	Performance compared to g-C$_3$N$_4$	Light source [a] (nm)	Reference (Year)
Li doped g-C$_3$N$_4$	2.8 times higher than that of g-C$_3$N$_4$	300 W, Visible light	[22] (2019)
Cl-S doped g-C$_3$N$_4$	5.3 times higher than that of g-C$_3$N$_4$	300 W, λ>400	[23] (2020)
Na doped g-C$_3$N$_4$	3.2 times higher than that of g-C$_3$N$_4$	500 W, λ>400	[24] (2020)
Na-S doped g-C$_3$N$_4$	3.4 times higher than that of g-C$_3$N$_4$	300 W, λ>420	[25] (2019)
Fe doped g-C$_3$N$_4$	2 times higher than that of g-C$_3$N$_4$	300 W, λ>420	[26] (2019)
K-Fe doped g-C$_3$N$_4$	4.38 times higher than that of g-C$_3$N$_4$	300 W, λ>420	[27] (2019)
C-Ce doped g-C$_3$N$_4$	2.4 times higher than that of g-C$_3$N$_4$	300 W, λ>420	[28] (2020)
P doped g-C$_3$N$_4$	5 times higher than that of g-C$_3$N$_4$	300 W, λ>420	[29] (2018)
Co doped g-C$_3$N$_4$/MoS$_2$	6.4 times higher than that of g-C$_3$N$_4$	300 W, simulated sunlight	[21] (2019)
Li-Cl-Co doped g-C$_3$N$_4$	**15.3 times higher than that of g-C$_3$N$_4$**	**300 W, simulated sunlight**	**This work**

Note: (a) the light source was a Xenon-arc lamp.

References

1. Q. Liu, Y. Guo, Z. Chen, Z. Zhang and X. Fang, Applied Catalysis B: Environmental, 2016, 183, 231-241.

2. G. Kresse, Furthm and J. Furthmüller, Physical Review B Condensed Matter, 1996, 54, 11169-11186.

3. G. Kresse and J. Furthmüller, Computational Materials Science, 1996, 6, 15-50.

4. B. PE, Physical Review B Condensed Matter, 1994, 50, 17953-17979.

5. J. P. Perdew, J. A. Chevary, S. H. Vosko, K. A. Jackson, M. R. Pederson, D. J. Singh and C. Fiolhais, Physical Review B Condensed Matter, 1993, 46, 6671-6687.

6. J. P. Perdew, K. Burke and M. Ernzerhof, Physical Review Letters, 1998, 77, 3865-3868.

7. S. Grimme, Journal of Computational Chemistry, 2006, 27, 1787-1799.

8. T. Xiong, W. Cen, Y. Zhang and F. Dong, ACS Catalysis, 2016, 6, 2462-2472.

9. X. Ma, Y. Lv, J. Xu, Y. Liu, R. Zhang and Y. Zhu, The Journal of Physical Chemistry C, 2012, 116, 23485-23493.

10. W. Zhang, Z. Zhang, S. H. Choi and W. Yang, Catalysis Today, 2019, 321-322, 67-73.

11. C. Liu, Y. Zhang, F. Dong, A. H. Reshak, L. Ye, N. Pinna, C. Zeng, T. Zhang and H. Huang, Applied Catalysis B: Environmental, 2017, 203, 465-474.

12. M. Xie, J. Tang, L. Kong, W. Lu, V. Natarajan, F. Zhu and J. Zhan, Chemical Engineering Journal, 2019, 360, 1213-1222.

13. X. She, L. Liu, H. Ji, Z. Mo, Y. Li, L. Huang, D. Du, H. Xu and H. Li, Applied Catalysis B: Environmental, 2016, 187, 144-153.

14. P. Chen, L. Chen, S. Ge, W. Zhang, M. Wu, P. Xing, T. B. Rotamond, H. Lin, Y. Wu and Y. He, International Journal of Hydrogen Energy, 2020, 45, 14354-14367.

15. S. Cao, Q. Huang, B. Zhu and J. Yu, Journal of Power Sources, 2017, 351, 151-159.

16. Y. Wang, S. Zhao, Y. Zhang, J. Fang, Y. Zhou, S. Yuan, C. Zhang and W. Chen, Applied Surface Science, 2018, 440, 258-265.

17. H. Che, C. Li, P. Zhou, C. Liu, H. Dong and C. Li, Applied Surface Science, 2020, 505, 144564.

18. Y. Cui, H. Wang, C. Yang, M. Li, Y. Zhao and F. Chen, Applied Surface Science, 2018, 441, 621-630.

19. J.-y. Tang, R.-t. Guo, W.-g. Pan, W.-g. Zhou and C.-y. Huang, Applied Surface Science, 2019, 467-468, 206-212.

20. J. Yang, Y. Liang, K. Li, G. Yang, K. Wang, R. Xu and X. Xie, Applied Catalysis B: Environmental, 2020, 262.

21. T. Chen, D. Yin, F. Zhao, K. K. Kyu, B. Liu, D. Chen, K. Huang, L. Deng and L. Li, New Journal of Chemistry, 2019, 43, 463-473.

22. W. Zhang, Z. Zhang, S. H. Choi and W. Yang, Catalysis Today, 2019, 321-322, 67-73.

23. F. Yi, H. Gan, H. Jin, W. Zhao, K. Zhang, H. Jin, H. Zhang, Y. Qian and J. Ma, Separation and Purification Technology, 2020, 233, 115997.

24. S. Wu, Y. Yu, K. Qiao, J. Meng, N. Jiang and J. Wang, Journal of Photochemistry and Photobiology A: Chemistry, 2020, DOI: https://doi.org/10.1016/j.jphotochem.2020.112999, 112999.

25. K.-L. Chen, S.-S. Zhang, J.-Q. Yan, W. Peng, D.-P. Lei and J.-H. Huang, International Journal of Hydrogen Energy, 2019, 44, 31916-31929.

26. T. Ma, Q. Shen, B. Z. J. Xue, R. Guan, X. Liu, H. Jia and B. Xu, Inorganic Chemistry Communications, 2019, 107, 107451.

27. W. Guo, J. Zhang, G. Li and C. Xu, Applied Surface Science, 2019, 470, 99-106.

28. K. Wu, D. Chen, S. Lu, J. Fang, X. Zhu, F. Yang, T. Pan and Z. Fang, Journal of Hazardous Materials, 2020, 382, 121027.

29. S. Liu, H. Zhu, W. Yao, K. Chen and D. Chen, Applied Surface Science, 2018, 430, 309-315.